Electronic Supplementary Material (ESI) for Physical Chemistry Chemical Physics.

Supporting information for: 2-Methoxyethanol: Harmonic tricks, anharmonic challenges and chirality-sensitive chain aggregation

Maxim Gawrilow and Martin A. Suhm*

Institut für Physikalische Chemie, Georg-August-Universität Göttingen, Tammannstr. 6, 37077 Göttingen, Germany

E-mail: msuhm@gwdg.de

Contents

1 Experimental details of double detection setup

A scheme of the new double detection setup is shown in Fig. S1. The Raman scattered light is collimated with a diameter of approx. 40 mm and exits the vacuum chamber from the left. At a 45° angle a dichroic mirror is mounted that either reflects or transmits the light, depending on its wavelength. In this work a shortpass mirror was used that transmits light with a wavelength that corresponds to a Raman Stokes shift of $<1600\,\mathrm{cm}^{-1}$, while reflecting light $>2050\,\mathrm{cm}^{-1}$. In order to cover the whole beam a rectangular filter of approx. 40 mm × 60 mm would be needed, but for economic reasons a filter with reduced size was employed (25.2 mm × 35.6 mm).

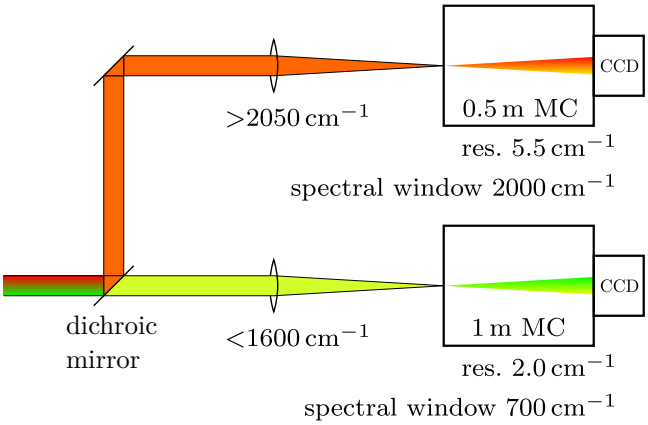

Fig. S1: Setup to separate the Raman scattering with a Stokes shift >2050 cm^{-1} (hydride stretches) from that with a Stokes shift <1600 cm^{-1} (fingerprint region).

Behind the dichroic filter the transmitted beam of scattered light is focussed on the entrance slit of a monochromator (1 m focal length), where a Stokes edge filter blocks off Rayleigh scattered light. A CCD camera at the exit detects the photons. The lower detection unit has a spectral window of 700 cm^{-1} and a resolution of 2 cm^{-1} when recording close to the Rayleigh line. For measurements in the OH stretching region without a dichroic mirror the spectral window reduces to 450 cm^{-1} and the resolution improves to 1.5 cm^{-1}.

The reflected light goes up and is further reflected towards a smaller monochromator (0.5 m focal length) that is mounted on top of the larger one. A focusing lens and a Raman edge filter are installed as well. The upper detection unit has a spectral window of 2000 cm^{-1} and a resolution of 5.5 cm^{-1}. A list of optical components used in the detection setup is given in Tab. S1.

The dichroic mirror reduced the signal intensity at the lower detection unit by only 7.5 %. According to the manufacturer specification, the intensity drop should increase for wavelengths close to the Rayleigh line at 532 nm. This effect was characterised by measuring two Raman spectra of 2-methoxyethanol close to the Rayleigh line with and without the dichroic mirror, the resulting spectra are shown in Fig. S2 together with the nominal filter transmission as

Tab. S1: List of optical components used in the new double detection setup

Component	Details
Light collection	camera objective (Canon); $f = 50\,\text{mm}$; aperture ratio 1.2
Mount system	60 mm optical cage system (Thorlabs)
Dichroic mirror	shortpass model HC BS 591 SP (AHF Anlagentechnik); $25.2\,\text{mm} \times 35.6\,\text{mm} \times 1.1\,\text{mm}$; transmission $<1600\,\text{cm}^{-1}$, reflection $>2050\,\text{cm}^{-1}$ (Stokes shift) at 45°. Alternatively, a longpass mirror is available: HC BS 624 (AHF Anlagentechnik); $25.2\,\text{mm} \times 35.6\,\text{mm} \times 2\,\text{mm}$; transmission $>2900\,\text{cm}^{-1}$, reflection $<2450\,\text{cm}^{-1}$ (Stokes shift).
Lower 1-m-MC	McPherson Inc. Model 2501; 1 m focal length; aperture ratio 8.7; ruled grating with 1200 grooves/mm
Focusing lens for 1-m-MC	ACH 25 x 225 VIS 0 TS (Edmund Optics) achromatic lens; $d = 25\,\text{mm}$; $f = 225\,\text{mm}$; aperture ratio 9
Detector on 1-m-MC	Princeton Instruments PyLoN400B; back-illuminated CCD with $1340\,\text{pixel} \times 400\,\text{pixel}$ (pixel dimensions: $20\,\mu\text{m} \times 20\,\mu\text{m}$); cryo-cooled to $-120\,°\text{C}$; quantum efficiency >95 % (600 nm)
Reflecting mirror for top part	BBE2-E02 (Thorlabs) dielectric elliptically shaped plane mirror; $50.8\,\text{mm} \times 71.8\,\text{mm}$
Upper 0.5-m-MC	McPherson Inc. Model 205f; 0.5 m focal length; aperture ratio 3.2; 600 grooves/mm
Focusing lens for 0.5-m-MC	AC254-080-A-ML (Thorlabs) achromatic lens; $d = 25.4\,\text{mm}$; $f = 80\,\text{mm}$; aperture ratio 3.15
Detector on 0.5-m-MC	Princeton Instruments Spec-10-400B; back-illuminated CCD with $1340\,\text{pixel} \times 400\,\text{pixel}$ (pixel dimensions: $20\,\mu\text{m} \times 20\,\mu\text{m}$); cryo-cooled to $-120\,°\text{C}$; quantum efficiency >90 % ((500–700) nm)

reported by the manufacturer. In contrast to the expectation no wavelength dependent loss of signal intensity is observed.

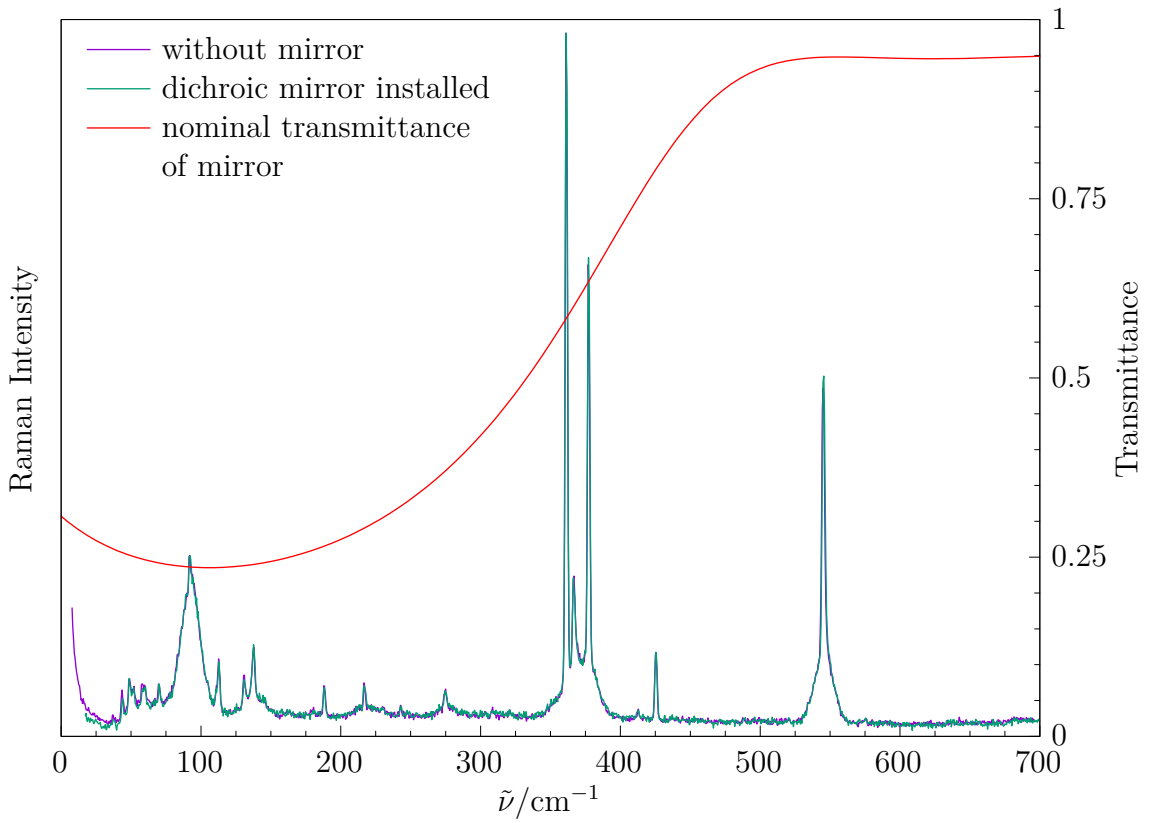

Fig. S2: Two low-frequency Raman spectra of methoxyethanol under identical conditions, once with and once without dichroic mirror installed, scaled to the signal at 361 cm^{-1}. Additionally, the transmittance of the dichroic mirror as specified by the manufacturer is shown. However, no effect of the mirror on the Raman spectrum is visible.

2 Area of detection

When recording spectra with two detection units it is necessary to ensure that both units are monitoring the same spot, i.e. they are receiving photons from a common region inside the supersonic expansion. This was investigated by recording the unbinned spectrum of a neon discharge lamp while a thin needle (width (0.40 ± 0.05) mm) being attached to the slit nozzle was positioned in the optical path. The results are shown in Fig. S3.

For the 1 m monochromator a sharp shadow with a height of ¼ of the total CCD chip height (400 px, pixel dimensions 20 µm × 20 µm) can be seen. Therefore the 1 m monochromator probes a region of (1.6 ± 0.2) mm height, which is significantly smaller than the slit nozzle

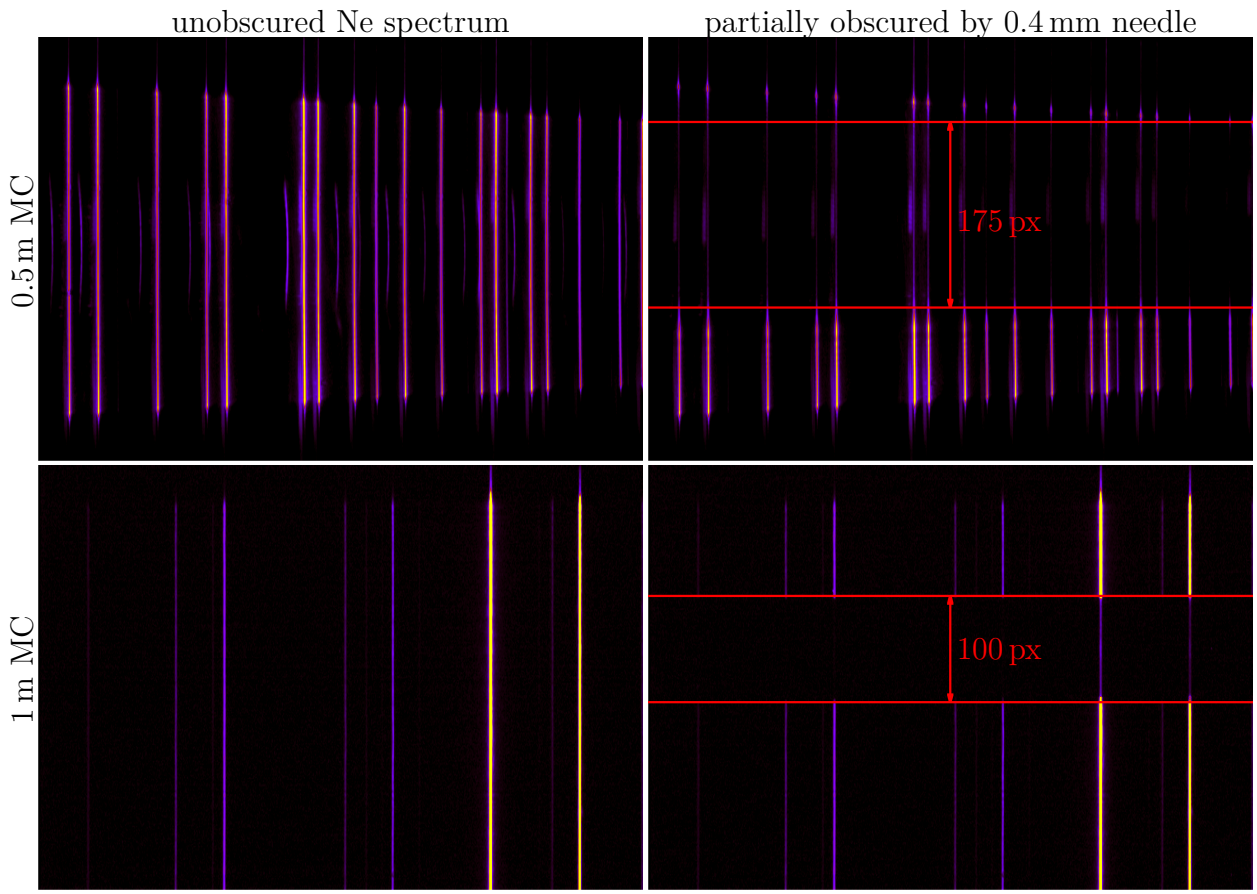

Fig. S3: 3D heat maps of a Ne spectrum obtained from simultaneous detection. On the left, the plain spectrum is shown. On the right, a small needle was attached to the slit nozzle and was moved into the optical pathway. The top picture corresponds to the 0.5 m monochromator, the bottom to the 1 m monochromator.

length (4 mm). Thereby it is ensured that always a small, homogenous central part of the expansion is detected.

Because a shadow can be simultaneously observed on the 0.5 m monochromator, it is proved that both monochromators are indeed capturing light from the same region in space. However, the 0.5 m monochromator is not strictly imaging, the vertical information gets partially scrambled, which can be seen by the blurred and sloped shadow. A rough estimate for the shadow height yields a probing height of approx. 0.9 mm.

3 Dependence of detection sensitivity on polarisation

The detection elements of the *curry*-jet, especially the CCD camera and the optical grating of the monochromator, are not equally sensitive to horizontally and vertically polarised light. This polarisation dependence is a function of the wavelength. In order to properly compare calculated Raman cross sections to experimental intensities, this function has to be determined.

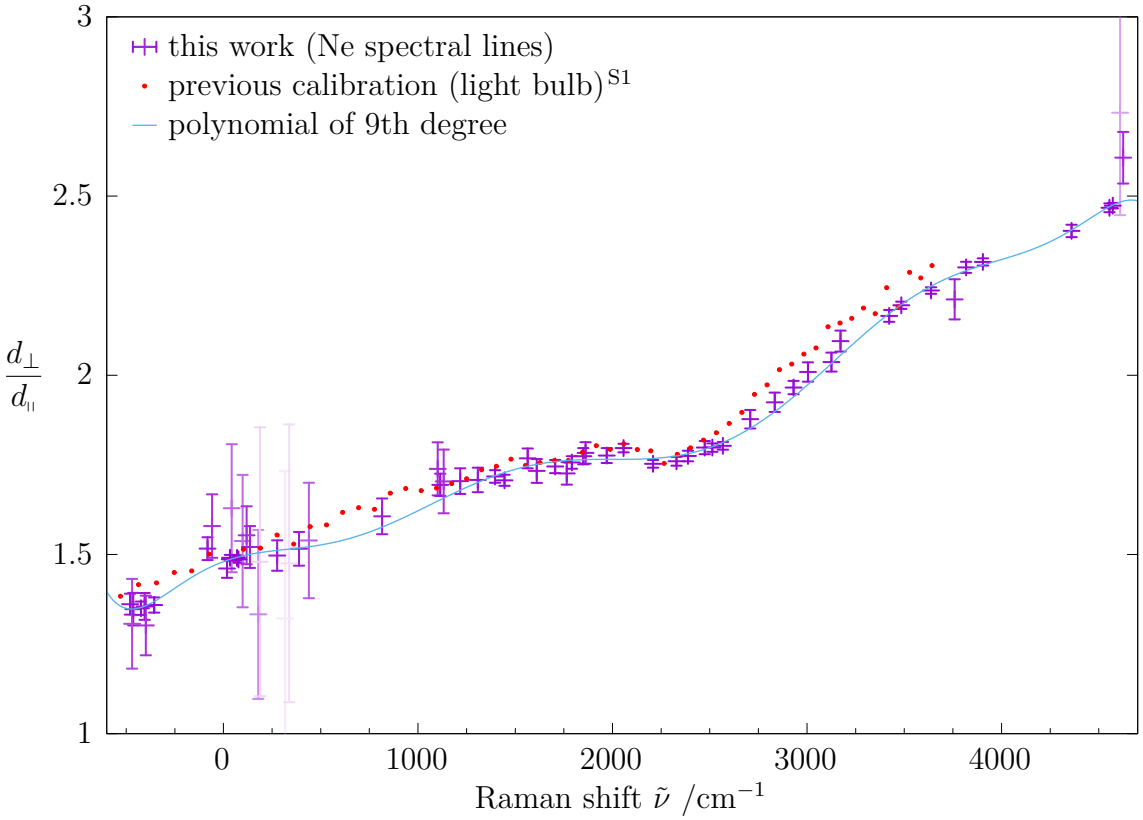

Fig. S4: Ratio of sensitivity for differently polarised light $^{d_\perp}/_{d_\parallel}$ for the 1 m monochromator (model 2501) and fitted polynomial of 9th degree. Data points with large error bars are shown more faintly due to their decreased weighting in the fit. The Raman shift $\tilde{\nu}$ is calculated for a laser wavelength of 532.27 nm.

In order to do so, spectral lines of an unpolarised light source (Ne discharge lamp, after checking its unpolarised character) were recorded at (500–700) nm with a polarisation filter (Thorlabs, LPVISE200-A, 50.8 mm, extinction coefficient 15000) being installed in front of the entrance slit of the 1 m monochromator. In combination with the 532 nm excitation

Tab. S2: Fitted coefficients of polynomial $P(\tilde{\nu}) = {}^{d_\perp}/_{d_\parallel} = \sum_{i=0}^{9} a_i(\tilde{\nu} - 2000\,\mathrm{cm}^{-1})^i$ that describes the ratio of detection sensitivity for orthogonal and parallel polarised light

a_i	$P(\tilde{\nu})$	
$/\mathrm{cm}^i$	a_i	Δa_i
a_0	1.7654	0.0034
a_1	0	
a_2	0	
$a_3 \cdot 10^{10}$	2.6970	0.1432
$a_4 \cdot 10^{13}$	0.4316	0.0622
$a_5 \cdot 10^{16}$	−1.1285	0.0991
$a_6 \cdot 10^{19}$	−0.1278	0.0267
$a_7 \cdot 10^{22}$	0.1926	0.0236
$a_8 \cdot 10^{26}$	0.1029	0.0274
$a_9 \cdot 10^{30}$	−1.1527	0.1867

laser, the lines cover Stokes shifts up to $4625\,\mathrm{cm}^{-1}$ and anti-Stokes shifts up to $480\,\mathrm{cm}^{-1}$. For perpendicular and parallel filter orientation w.r.t. the grating lines five measurements each were recorded in an alternating fashion. First-order baseline correction was achieved by subtracting the median of each individual spectrum, signals were integrated over ±7 px around the peak maximum. For each set of five measurements the mean value and sample standard deviation were determined, and from these mean values the ratio of sensitivity was calculated. For all wavelengths the detection sensitivity for perpendicularly polarised light $d_\perp$ was larger than for parallel $d_\parallel$. The error of the ratio ${}^{d_\perp}/_{d_\parallel}$ was calculated by maximum error propagation and was used as weighting factor for the fitting of a polynomial. Empirically it was found that a polynomial of 9th degree gives a sufficient description. The zero point of the polynomial was shifted to $2000\,\mathrm{cm}^{-1}$, the center of the range of interest. Furthermore it was found that setting the first and second term to zero gives best interpolation results with smallest uncertainties for the coefficients. The results are shown in Fig. S4 and Tab. S2. Coefficients were rounded such that the shape of the polynomial was preserved. They are consistent with older calibration data that had been obtained with a light bulb, a polarisation filter of unknown quality (Hama Hoya 450/670) and a different CCD camera (Spec-10-400B).[S1] For

these measurements, the Raman edge filter was removed, however, it was observed that it had no effect on the polarisation sensitivity.

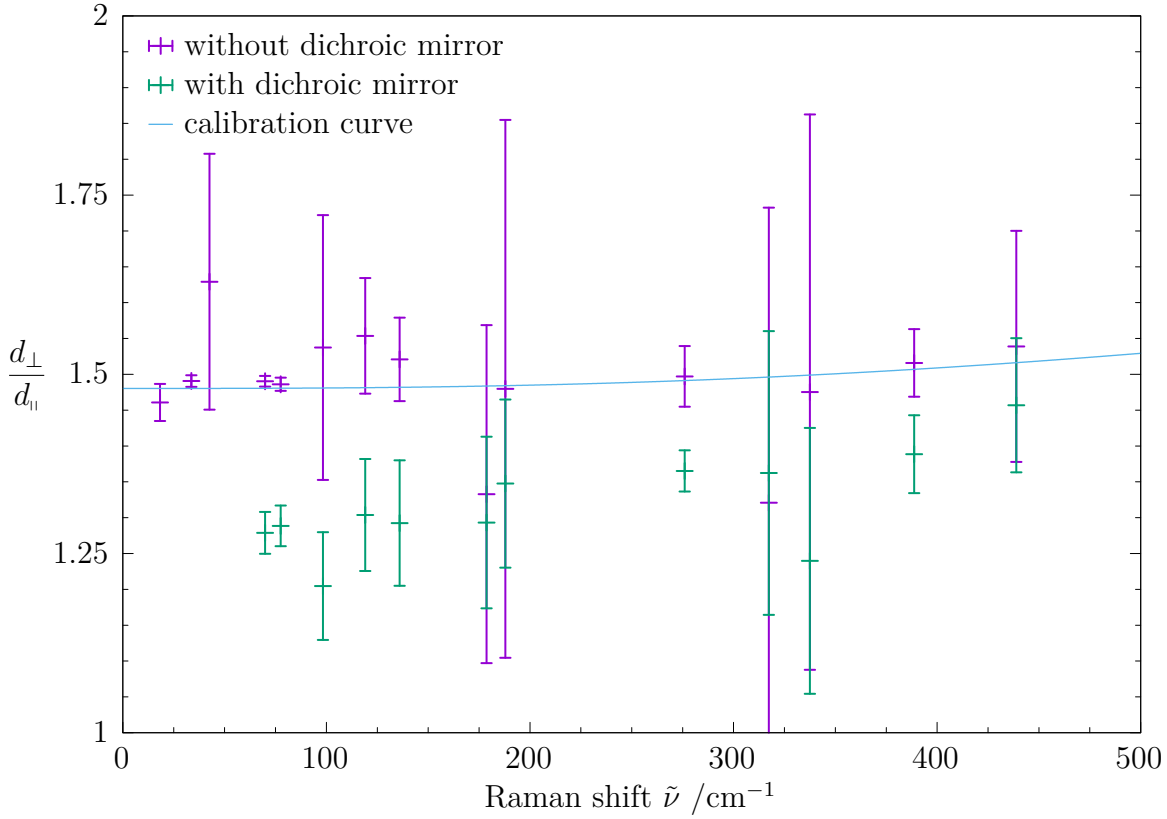

Fig. S5: Ratio of sensitivity for differently polarised light recorded with and without the dichroic mirror in transmission mode, and the calibration curve from Fig. S4.

The influence of the dichroic beamsplitter on the sensitivity ratio was investigated as well, the results are shown in Fig. S5. Only small changes can be observed. Because data obtained with the double detection setup are to be interpreted only qualitatively, it is acceptable to use the calibration curve from Tab. S2 for all calculated spectra. If a quantitative analysis of signal intensities was to be made, a separate calibration curve would be required.

The ratio of sensitivity for the upper detection unit (monochromator length 0.5 m, dichroic mirror installed, polarisation filter in front of entrance slit of monochromator) is shown in Fig. S6. Compared to the lower detection unit the ratio of sensitivity is much closer to unity.

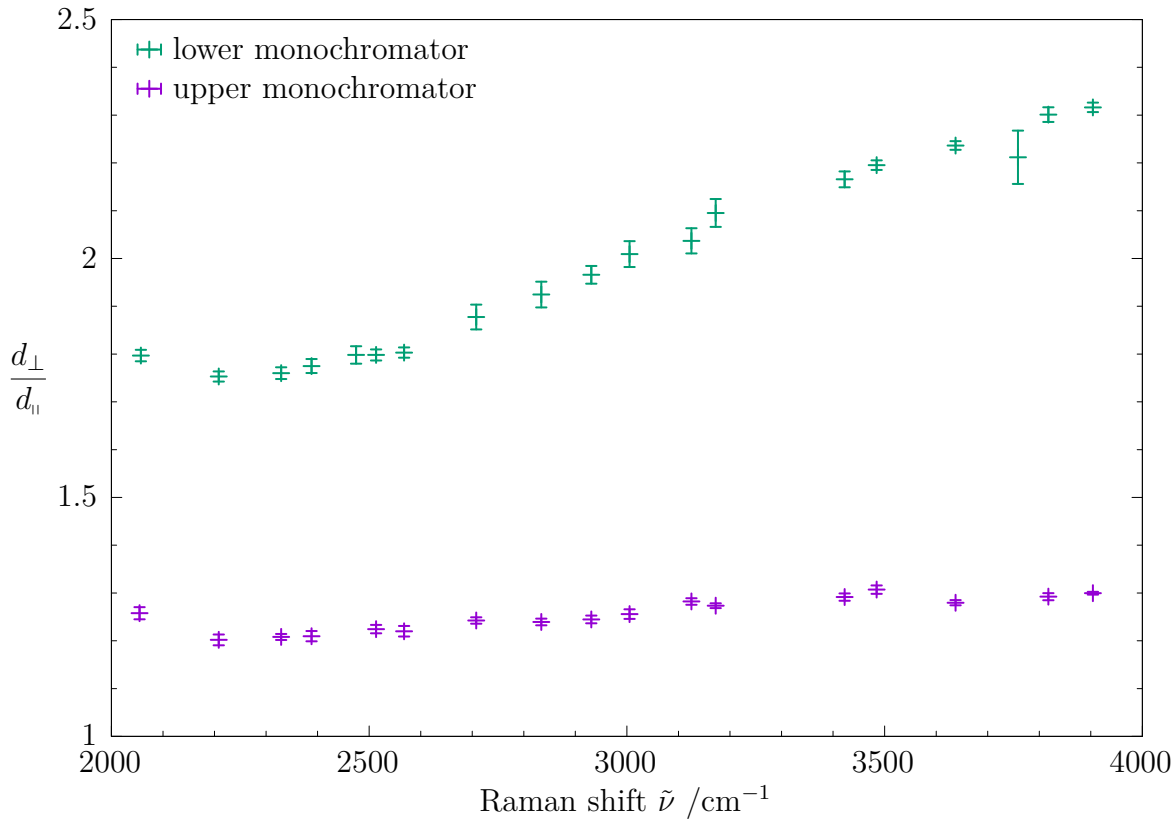

Fig. S6: Ratio of sensitivity for differently polarised light for the upper (0.5 m) and lower (1 m) monochromator.

4 Additional Raman spectra

The full spectrum of 2-methoxyethanol including the C−H stretching region obtained with the upper detection unit is provided in Fig. S7. Fig. S8 shows how the fully polarised part is obtained experimentally. The full list of observed Raman signals together with their assignment is given in Tab. S3.

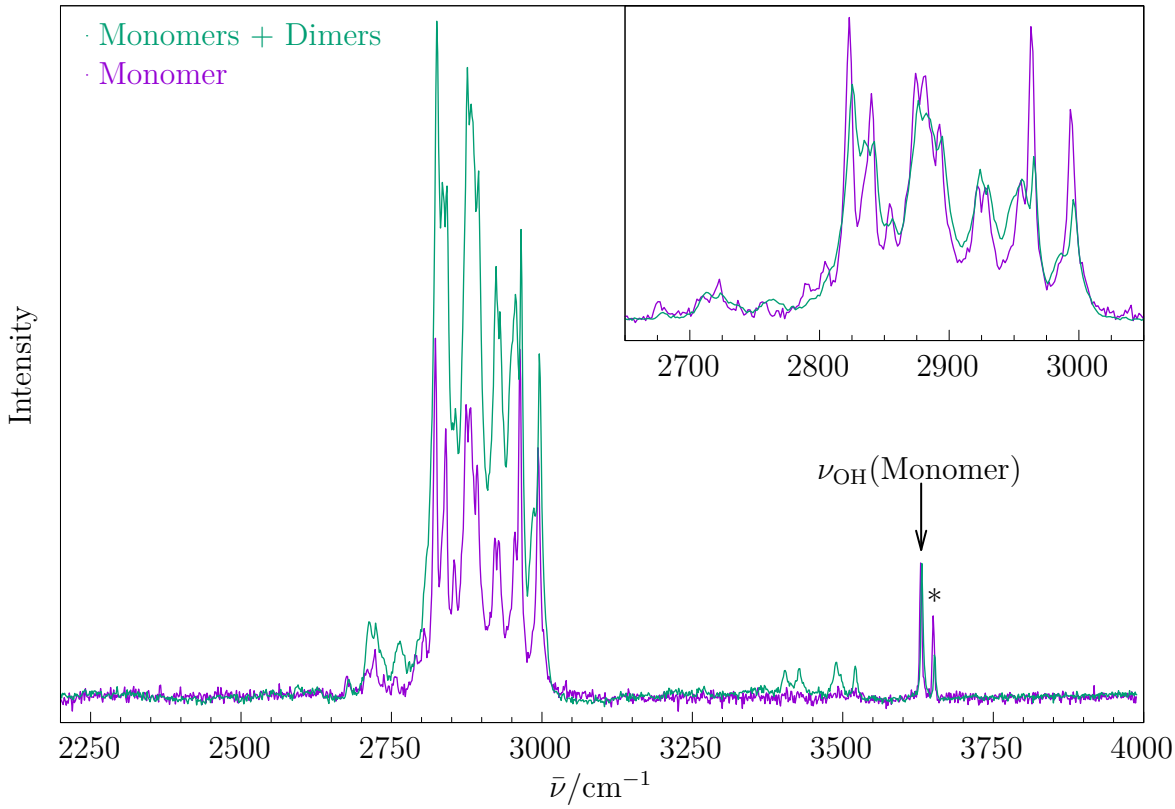

Fig. S7: Raman spectra of 2-methoxyethanol under different conditions. The main spectra are scaled to equal monomer OH stretch signal at $3635\,\mathrm{cm}^{-1}$, in the top right inlet the spectra are scaled to the integrated CH-stretch-region ($(2650–3050)\,\mathrm{cm}^{-1}$). Water signal is marked by a *. Experimentally, assuming that average scattering cross sections in the CH region are not significantly affected by dimerisation, these spectra give an average Raman OH stretching visibility for cold dimers which is 3–4 times larger than for monomers. The harmonic calculations predict a factor of about 5, which is reasonably consistent with experiment, given the approximations involved in the calculation.

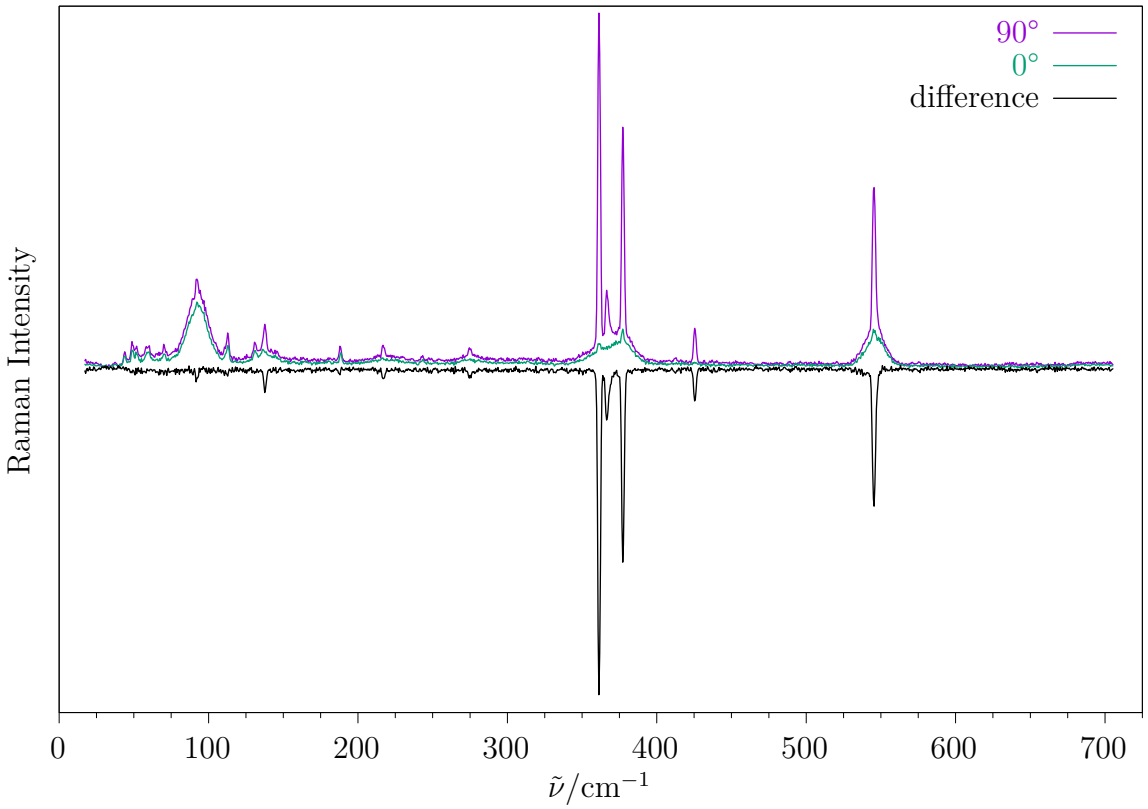

Fig. S8: Exemplary Raman spectra that demonstrate how the fully polarised part is obtained. Two Raman spectra of 2-methoxyethanol were recorded under identical conditions, once with the incident laser polarisation at 90° to the scattering plane, once with 0°. The totally polarised part is expected to be close to $I(90°) - 7/6 \cdot I(0°)$, but due to unequal sensitivity for differently polarised light and collection of the light from a cone of different scattering angles the empirical factor of 1.195 instead of $7/6$ is used. The same factor is used for calculated Raman cross sections.

Tab. S3: Observed wavenumbers and assignments

Species	wavenumber /cm^{-1}	assignment	dominant motion
gG'T	92	ν_{33}	OMe torsion
	137	ν_{32}	skeletal
	217	ν_{31}	CH_3 torsion
	275	ν_{30}	skeletal
	361	ν_{29}	skeletal
	366	$\nu_{33} + \nu_{30}$	
	377	ν_{28}	OH torsion
	545	ν_{27}	skeletal
	3635	ν_1	OH stretch
gTT	425	ν_{28}	skeletal accordion
	3656	ν_1 (and H_2O)	OH stretch
Dimers	$<$ 150		
	161		
	180		
	227		
	368		
	498		OH torsion
	520		OH torsion
	535		
	3409	het-c	OH stretch
	3432	hom-c	OH stretch
	3490–3500	hom-r C_2, hom-c', het-c'	OH stretch
	3524	het-r C_i	OH stretch

5 Keywords for calculations with Turbomole and Gaussian

Structure optimisation, harmonic frequency analysis and Raman cross sections were calculated with Turbomole[S2] on MARIJ-B3LYP-D3(BJ,abc)/def2-QZVPP level[S3–S8]. The integration grid m5, Grimme's dispersion correction D3[S9] with Becke-Johnson-damping[S10] and three-body terms, resolution of the identity for the Coulomb part RI-J[S11–S14] and multipole accelerated resolution of the identity MARI-J[S15] were used. Since Turbomole uses mean isotope masses as default, these were changed to the mass of the main isotope: H 1.007 825 03 u, C 12 u, O 15.994 914 62 u. For all other parameters the default values were used. Preoptimisation was done with the B97-3c functional[S16], for which the modified def2-mTZVP basis set, grid m5, dispersion correction D3(BJ,abc) and RI-J were employed.

Raman cross sections $\sigma(i)$ of normal mode i with wavenumber $\tilde{\nu}_i$ were calculated for a laser wavelength $\lambda_{\text{laser}} = 532.27\,\text{nm}$, vibrational temperature $T = 100\,\text{K}$, taking into account detection sensitivity for differently polarised light *via* the polynomial $P(\tilde{\nu})$ (see Tab. S2) and that the setup is counting photons.[S1] Turbomole output contains derivatives of isotropic and anisotropic polarisability α' and γ' in atomic units ($a_0{}^2 m_\text{e}{}^{-0.5}$), which are transferred to Raman cross sections *via* Eq. 1 for orthogonal polarisation of incident laser radiation and *via* Eq. 2 for parallel polarisation. The resulting Raman cross sections are typically in the order of $10^{-35}\,\text{m}^2\,\text{sr}^{-1}$.

$$\sigma_\perp(i) = \frac{2\pi^2 h\tilde{\nu}_\text{laser}}{45c} \cdot \frac{(\tilde{\nu}_\text{laser} - \tilde{\nu}_i)^3}{\tilde{\nu}_i \left(1 - \exp\left(-\frac{hc\tilde{\nu}_i}{k_B T}\right)\right)} \cdot \left(45\alpha_i'^2 + 4\gamma_i'^2 + \frac{3\gamma_i'^2}{P(\tilde{\nu}_i)}\right) \tag{1}$$

$$\sigma_\shortparallel(i) = \frac{2\pi^2 h\tilde{\nu}_\text{laser}}{45c} \cdot \frac{(\tilde{\nu}_\text{laser} - \tilde{\nu}_i)^3}{\tilde{\nu}_i \left(1 - \exp\left(-\frac{hc\tilde{\nu}_i}{k_B T}\right)\right)} \cdot \left(3\gamma_i'^2 + \frac{3\gamma_i'^2}{P(\tilde{\nu}_i)}\right) \tag{2}$$

Single point energies on CCSD(T)-F12 level[S17] were calculated with Turbomole using the cc-pVTZ-F12 basis set, a SCF convergence threshold of $1 \cdot 10^{-9}\,E_\mathrm{h}$, frozen core orbitals and resolution of the identity for both Coulomb and exchange part RI-JK[S18]. Explicit correlation was included as (F12*) approximation[S19] with ansatz 2 and r12model B. The corresponding auxiliary basis sets `cbas`, `cabs` and `jkbas` were used. All other parameters were kept at their default values.

Anharmonic VPT2 calculations were performed with Gaussian09[S20] and Gaussian16[S21] using B3LYP[S3–S8] and PBE0[S3,S4,S22–S24] functionals and def2-TZVPP and def2-QZVPP basis sets. The keyword input line for B3LYP/def2-QZVPP is identical for both program versions:

```
# b3lyp def2qzvpp Int=SuperFine SCF(Conver=10) empiricaldispersion=gd3bj
opt=(VeryTight,MaxCycles=300) freq=anharmonic
```

6 Calculated dimer energies

A list of all 23 dimers that were found by the automated structure search is given in Tab. S4. Dimers that consist of different conformers and are bound in a concerted fashion are named according to their structure: The hydrogen bond from the first conformer binds to the OH group of the second, whereas the hydrogen bond from the second conformer binds to the ether-O of the first one.

Tab. S4: Relative dimer energies in kJ/mol on RIJK-CCSD(F12*)(T*)/cc-pVTZ-F12//MARIJ-B3LYP-D3(BJ,abc)/def2-QZVPP level, without (E_{el}) and with B3LYP ZPE included (E_{ZPE}). In parentheses, the results without CCSD(T) correction are given

Conformer	E_{el}		E_{ZPE}	
het-c	0	(0)	0	(0)
hom-r C_2	2.8	(1.7)	1.4	(0.3)
het-r C_i	2.2	(1.9)	1.1	(0.8)
hom-c	2.5	(2.0)	1.5	(0.9)
het-r'	2.9	(2.6)	1.9	(1.6)
hom-r' C_2	3.5	(3.0)	2.2	(1.8)
het-c'	4.1	(3.5)	2.9	(2.3)
gG'T-g'GG r	4.8	(3.5)	4.6	(3.3)
hom-c'	5.8	(5.0)	4.7	(3.9)
hom-c"	6.0	(5.7)	4.3	(4.1)
gG'T-gG'G r	6.5	(5.5)	5.9	(4.9)
gG'T-g'GG c	5.7	(5.1)	5.6	(5.0)
gG'T-gG'G' c	6.4	(5.9)	6.4	(5.9)
gG'T-g'G'T r	7.1	(7.1)	5.9	(6.0)
gG'T-gG'G' r	7.8	(7.2)	7.3	(6.6)
gG'G'-gG'T c	7.7	(7.0)	7.5	(6.8)
g'GG-gG'T c	8.0	(7.7)	7.6	(7.2)
gG'T-g'GG c	8.4	(7.5)	8.2	(7.3)
g'GG-gG'T c	10.0	(8.7)	9.2	(8.0)
gG'T-gG'G' c	10.7	(9.6)	10.1	(9.0)
gG'T-gGG r	10.8	(10.2)	10.2	(9.5)
gG'G'-gG'T c	11.4	(10.8)	10.2	(9.6)
gG'T-gGG c	11.4	(10.3)	11.1	(10.0)

7 Figures of calculated monomer and dimer structures

Graphical representation of the observed and assigned monomer structures (gG'T and gTT) as well as the ten most stable dimer structures that were found by the automated conformer search, optimised on MARIJ-B3LYP-D3(BJ,abc)/def2-QZVPP level. Dimers that were assigned experimentally are labeled in bold. For some PDF viewers (e.g. Adobe Reader), interactive 3D graphics may be available, for others only a static screenshot is displayed. The dimer descriptors Dxy correspond to the file names of .xyz files that are supplied in a separate .tar.xz archive. These coordinate files may be used instead to obtain a spatial impression.

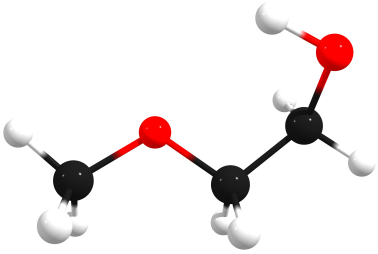

gG'T

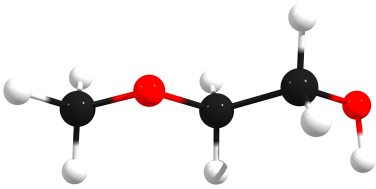

gTT

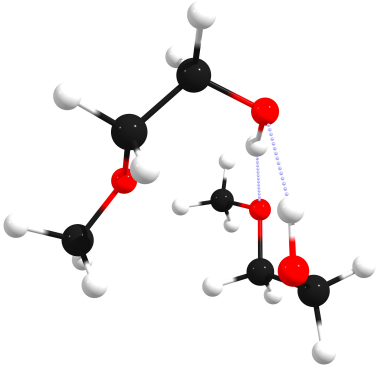

D01 het-c

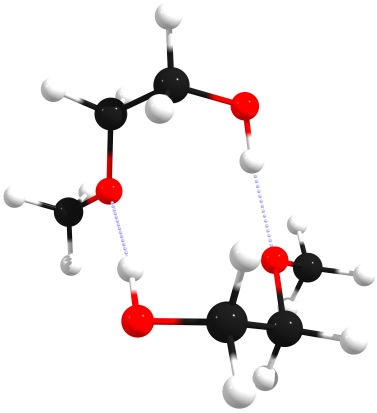

D02 hom-r (C_2)

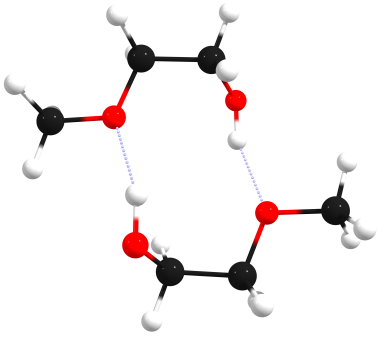

D03 het-r (C_i)

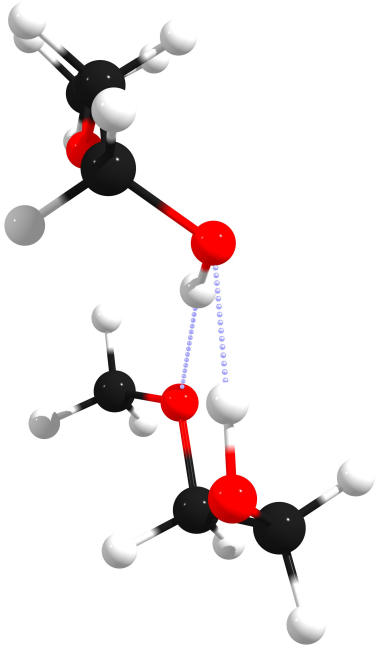

D04 hom-c

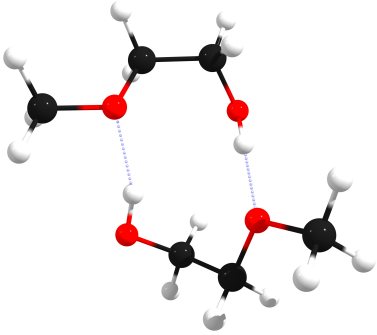

D05 het-r'

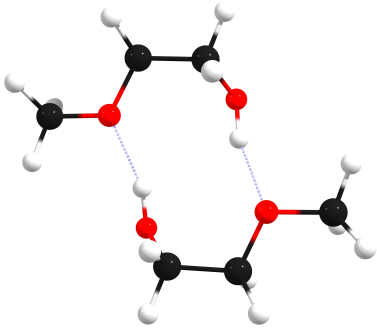

D06 hom-r' (C_2)

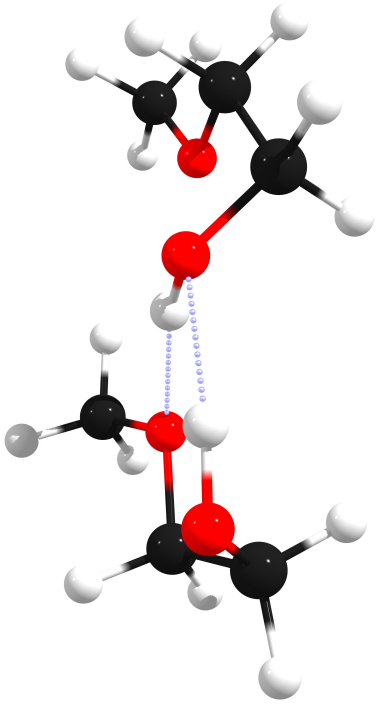

D07 het-c’

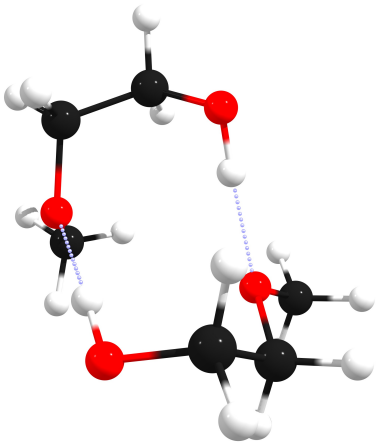

D08 gG’T+g’GG-r

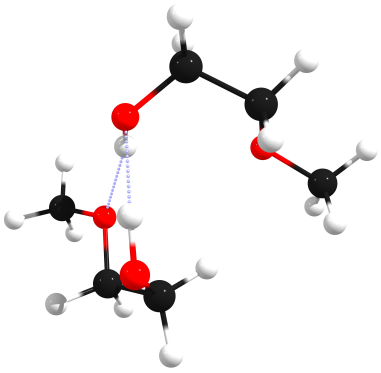

D09 hom-c’

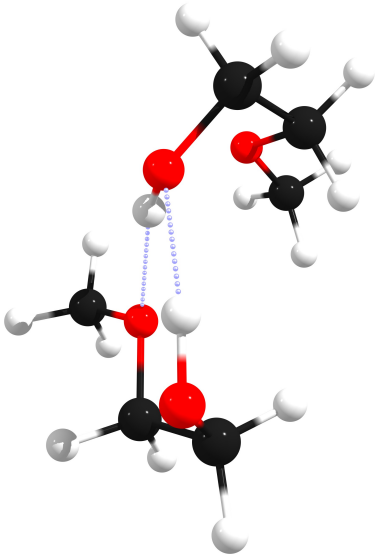

D10 hom-c”

8 Lists of VPT2 results for gG’T

Results of anharmonic VPT2 calculations for gG’T with Gaussian09 and Gaussian16 are provided. Fundamentals obtained with B3LYP are listed in Tab. S5, those obtained with

PBE0 in Tab. S6. Overtones are given in Tab. S7. Combination modes obtained with B3LYP are listed in Tab. S8, those obtained with PBE0 in Tab. S9.

Tab. S5: Fundamentals calculated with G16 and G09 on B3LYP/def2-QZVPP and def2-TZVPP level. Harmonic wavenumber ν_h, anharmonic wavenumber ν_{ah} in cm^{-1}, harmonic infrared intensity I_h, anharmonic infrared intensity I_{ah} in $km\,mol^{-1}$

	Gaussian 16								Gaussian 09							
	QZ				TZ				QZ				TZ			
Mode	ν_h	ν_{ah}	I_h	I_{ah}	ν_h	ν_{ah}	I_h	I_{ah}	ν_h	ν_{ah}	I_h	I_{ah}	ν_h	ν_{ah}	I_h	I_{ah}
33	92	146	1	1	91	111	1	1	92	88	1	1	91	88	1	1
32	137	82	7	0	139	49	7	1	137	132	7	6	139	135	7	6
31	224	319	5	9	224	291	5	8	224	211	5	5	224	213	5	5
30	277	277	3	6	277	262	3	9	277	273	3	3	277	273	3	3
29	367	362	14	22	368	300	11	79	367	359	14	25	368	364	11	25
28	407	443	113	35	413	432	119	32	407	362	113	87	413	367	119	97
27	548	547	6	8	548	542	6	3	548	543	6	5	548	542	6	3
26	840	817	20	9	841	826	20	18	840	826	20	20	841	827	20	21
25	904	892	15	25	906	887	15	21	904	885	15	17	906	886	15	17
24	1023	1005	15	16	1024	1001	15	15	1023	1001	15	14	1024	1002	15	14
23	1076	1054	120	128	1078	1049	117	121	1076	1046	120	118	1078	1048	117	116
22	1123	1103	8	8	1124	1100	8	7	1123	1099	8	8	1124	1100	8	7
21	1150	1119	127	120	1152	1116	126	123	1150	1113	127	126	1152	1116	126	128
20	1184	1161	2	2	1183	1157	2	2	1184	1159	2	2	1183	1158	2	2
19	1197	1173	31	20	1197	1171	33	20	1197	1170	31	19	1197	1171	33	21
18	1254	1222	13	7	1254	1219	12	7	1254	1224	13	11	1254	1225	12	11
17	1271	1251	21	23	1270	1243	22	16	1271	1238	21	18	1270	1239	22	19
16	1378	1340	4	0	1379	1335	5	0	1378	1341	4	7	1379	1343	5	8
15	1403	1372	27	12	1403	1368	29	9	1403	1371	27	21	1403	1371	29	20
14	1434	1405	28	34	1435	1401	31	22	1434	1392	28	18	1435	1394	31	21
13	1478	1437	1	5	1478	1439	1	1	1478	1444	1	2	1478	1444	1	2
12	1490	1451	8	6	1489	1447	8	4	1490	1450	8	6	1489	1447	8	4
11	1498	1456	8	3	1499	1450	10	2	1498	1457	8	7	1499	1457	10	8
10	1500	1471	5	8	1501	1467	3	8	1500	1460	5	4	1501	1460	3	2
9	1515	1486	4	3	1516	1482	4	3	1515	1476	4	3	1516	1476	4	3
8	2962	2849	39	45	2966	2839	37	24	2962	2823	39	18	2966	2825	37	123
7	2978	2783	76	22	2981	2784	76	16	2978	2802	76	82	2981	2802	76	34
6	2987	2836	1	25	2990	2833	2	23	2987	2843	1	69	2990	2847	2	4
5	3007	2862	121	60	3010	2866	121	68	3007	2865	121	32	3010	2866	121	80
4	3020	2894	38	3	3023	2893	40	4	3020	2876	38	12	3023	2881	40	19
3	3082	2948	30	36	3085	2949	31	35	3082	2945	30	35	3085	2947	31	36
2	3113	2976	25	27	3116	2977	26	29	3113	2975	25	26	3116	2977	26	29
1	3804	3624	38	45	3806	3620	36	29	3804	3621	38	31	3806	3621	36	29

Tab. S6: Fundamentals calculated with G16 and G09 on PBE0/def2-QZVPP and def2-TZVPP level. Harmonic wavenumber ν_{h}, anharmonic wavenumber ν_{ah} in $\mathbf{cm^{-1}}$, harmonic infrared intensity I_{h}, anharmonic infrared intensity I_{ah} in $\mathbf{km\,mol^{-1}}$

	Gaussian 16								Gaussian 09							
	QZ				TZ				QZ				TZ			
Mode	ν_{h}	ν_{ah}	I_{h}	I_{ah}	ν_{h}	ν_{ah}	I_{h}	I_{ah}	ν_{h}	ν_{ah}	I_{h}	I_{ah}	ν_{h}	ν_{ah}	I_{h}	I_{ah}
33	94	147	1	1	93	111	1	1	94	90	1	1	93	90	1	1
32	137	80	7	0	139	50	7	1	137	132	7	6	139	133	7	6
31	226	320	5	7	226	290	5	8	226	212	5	5	226	213	5	5
30	278	279	3	6	278	261	3	9	278	274	3	3	278	273	3	3
29	367	357	14	31	369	297	11	66	367	361	14	26	369	362	11	18
28	412	444	112	31	417	438	118	41	412	367	112	86	417	372	118	96
27	551	550	6	7	551	545	6	4	551	545	6	4	551	545	6	3
26	852	847	17	14	853	839	18	16	852	839	17	18	853	839	18	19
25	917	905	11	20	918	900	12	16	917	899	11	13	918	900	12	13
24	1046	1028	17	15	1047	1024	17	15	1046	1024	17	16	1047	1025	17	16
23	1103	1081	99	79	1104	1078	97	108	1103	1077	99	106	1104	1078	97	104
22	1135	1115	29	52	1135	1110	30	21	1135	1110	29	21	1135	1111	30	21
21	1182	1157	32	85	1182	1156	20	15	1182	1155	32	122	1182	1156	20	69
20	1187	1162	30	31	1187	1153	37	101	1187	1161	30	19	1187	1161	37	37
19	1209	1182	99	49	1210	1182	103	38	1209	1177	99	57	1210	1177	103	63
18	1261	1226	14	8	1261	1224	13	7	1261	1230	14	10	1261	1230	13	11
17	1272	1253	23	5	1272	1248	24	18	1272	1243	23	1	1272	1241	24	16
16	1378	1341	1	1	1379	1339	1	1	1378	1344	1	3	1379	1345	1	3
15	1398	1364	29	13	1399	1360	30	10	1398	1365	29	23	1399	1366	30	25
14	1438	1411	31	30	1439	1408	34	29	1438	1399	31	15	1439	1400	34	16
13	1471	1439	1	2	1472	1436	1	2	1471	1439	1	1	1472	1439	1	3
12	1483	1445	9	5	1482	1443	9	5	1483	1443	9	5	1482	1443	9	5
11	1490	1443	10	1	1492	1442	11	1	1490	1451	10	65	1492	1451	11	44
10	1493	1466	4	8	1494	1464	3	6	1493	1456	4	63	1494	1456	3	76
9	1510	1480	6	5	1511	1479	5	3	1510	1472	6	4	1511	1473	5	4
8	2979	2843	36	5	2982	2841	34	4	2979	2839	36	128	2982	2840	34	163
7	2993	2800	72	27	2996	2797	71	17	2993	2814	72	66	2996	2816	71	35
6	3004	2856	7	10	3006	2853	9	8	3004	2855	7	8	3006	2857	9	7
5	3026	2891	111	176	3029	2889	111	171	3026	2900	111	145	3029	2900	111	150
4	3044	2927	35	5	3047	2923	37	8	3044	2911	35	32	3047	2912	37	33
3	3102	2972	27	30	3105	2972	29	32	3102	2967	27	32	3105	2969	29	33
2	3135	3001	22	26	3138	3001	23	27	3135	2999	22	26	3138	3001	23	26
1	3855	3676	42	48	3857	3673	40	34	3855	3674	42	35	3857	3674	40	34

Tab. S7: Overtones calculated with G16 and G09 using B3LYP/PBE0 and def2-QZVPP/def2-TZVPP level. Harmonic wavenumber ν_h, anharmonic wavenumber ν_{ah} in cm^{-1}, anharmonic infrared intensity I_{ah} in km mol^{-1}. Only listed if intensity exceeds 1 km mol^{-1}. Note that the differences between G09 and G16 for overtones (and combination modes) can be much smaller than for the underlying fundamentals in some cases, perhaps indicating unrealistic default settings for (1,1)-Darling-Dennison thresholds as one possible cause of discrepancy to experiment.

	Gaussian 16						Gaussian 09					
	B3LYP/QZ			B3LYP/TZ			B3LYP/QZ			B3LYP/TZ		
Mode	ν_h	ν_{ah}	I_{ah}	ν_h	ν_{ah}	I_{ah}	ν_h	ν_{ah}	I_{ah}	ν_h	ν_{ah}	I_{ah}
28	815	842	13	826	693	4	815	684	4	826	692	4
27	1096	1093	1	1097	1084	1	1096	1084	1	1097	1084	1
16	2756	2680	1	2759	2672	1	2756	2669	1	2759	2672	1
15	2806	2733	3	2806	2728	3	2806	2730	2	2806	2730	2
14	2867	2785	2	2870	2780	2	2867	2777	3	2870	2779	3
13	2956	2905	11	2956	2907	10	2956	2903	1	2956	2896	12
12	2981	2891	3	2977	2880	14	2981	2885	2	2977	2884	1
11	2997	2919	8	2998	2909	4	2997	2936	4	2998	2910	0
10	3001	2925	3	3001	2932	8	3001	2911	1	3001	2936	17
9	3031	2974	11	3032	2965	10	3031	2959	2	3032	2959	2
1	7609	7073	3	7612	7062	3	7609	7067	3	7612	7064	3
	PBE0/QZ			PBE0/TZ			PBE0/QZ			PBE0/TZ		
28	824	815	6	835	702	4	824	692	4	835	703	5
27	1101	1098	1	1102	1089	1	1101	1089	1	1102	1089	1
16	2755	2684	1	2759	2679	1	2755	2675	1	2759	2678	1
15	2796	2722	2	2797	2717	2	2796	2717	1	2797	2718	1
14	2876	2789	2	2879	2786	2	2876	2782	2	2879	2785	2
13	2943	2902	3	2943	2898	2	2943	2906	1	2943	2908	2
12	2965	2888	15	2964	2885	15	2965	2876	12	2964	2875	8
11	2981	2909	15	2983	2907	5	2981	2889	5	2983	2890	3
10	2987	2925	1	2989	2925	3	2987	2914	3	2989	2921	9
9	3019	2960	28	3022	2957	25	3019	2955	14	3022	2957	12
1	7709	7178	2	7714	7171	3	7709	7175	2	7714	7173	3

Tab. S8: Combination modes calculated with G16 and G09 on B3LYP/def2-QZVPP and def2-TZVPP level. Harmonic wavenumber ν_{h}, anharmonic wavenumber ν_{ah} in cm^{-1}, anharmonic infrared intensity I_{ah} in $\mathrm{km\,mol}^{-1}$. Only listed if intensity exceeds $1\,\mathrm{km\,mol}^{-1}$

B3LYP/def2-QZVPP								B3LYP/def2-TZVPP							
		G16			G09					G16			G09		
Modes		ν_{h}	ν_{ah}	I_{ah}	ν_{h}	ν_{ah}	I_{ah}	Modes		ν_{h}	ν_{ah}	I_{ah}	ν_{h}	ν_{ah}	I_{ah}
33	32	229	311	2				32	28	552	502	2	552	501	2
33	31	316	382	1				28	27	961	909	2	961	909	2
33	30	369	430	8	369	362	6	31	26	1066	1038	1	1066	1039	1
32	30	414	454	17				30	26	1119	1100	3	1119	1099	3
28	27	955	984	2	955	904	1	32	24	1163	1138	7	1163	1138	7
31	26	1064	1063	1	1064	1036	1	29	26	1209	1188	4	1209	1188	4
30	26	1118	1115	3	1118	1098	3	28	26	1254	1194	2	1254	1193	2
31	25	1129	1125	1	1129	1098	1	29	25	1273	1251	8			
32	24	1160	1172	9	1160	1134	9	32	18	1393	1359	1	1393	1359	1
30	25	1182	1175	1	1182	1158	1	29	24	1392	1363	1	1392	1363	1
29	26	1207	1204	5	1207	1184	5	30	22	1401	1374	4	1401	1373	4
29	25	1271	1265	2				29	23	1446	1415	14			
28	26	1247	1266	1				27	25	1454	1428	1	1454	1428	1
32	21	1287	1283	1	1287	1246	1	31	18	1479	1435	2			
30	22	1400	1389	2	1400	1372	2	29	22	1492	1463	3	1492	1463	3
29	23	1442	1429	3				26	21	1993	1937	2	1993	1938	2
27	25	1452	1436	1	1452	1427	1	24	21	2176	2110	2	2176	2111	2
26	21	1990	1943	2	1990	1934	2	16	14	2814	2727	1	2814	2727	1
24	21	2173	2117	2	2173	2107	2	15	14	2838	2751	1	2838	2751	1
15	14	2837	2755	1	2837	2749	1	15	13	2881	2810	1	2881	2810	1
15	13	2881	2816	2	2881	2810	2	14	13	2913	2838	1	2913	2838	1
12	10				2991	2918	3	14	11	2934	2852	1	2934	2853	1
14	13	2912	2844	2	2912	2837	2	14	10	2936	2855	1	2936	2855	1
15	9	2919	2849	1	2919	2843	1	14	9	2951	2870	5	2951	2870	5
14	11	2932	2858	1	2932	2851	1	13	12	2966	2883	32	2966	2883	32
14	9	2949	2875	6	2949	2869	6	12	11	2987	2898	6	2987	2898	6
13	12	2968	2890	13	2968	2886	13	13	11	2977	2898	23	2977	2898	23
13	11	2977	2907	1				13	10	2978	2903	2			
12	11	2989	2910	10	2989	2905	10	12	10	2989	2916	1			
12	9	3006	2925	98	3006	2920	97	11	10	2999	2918	15	2999	2919	6
13	9	2994	2929	3				12	9	3005	2919	15	3005	2919	15
11	10	2999	2935	11	2999	2928	5	13	9	2994	2922	3			
11	9	3014	2944	11	3014	2937	11	11	9	3015	2938	34	3015	2939	35
10	9	3016	2949	9	3016	2942	12	10	9	3017	2943	11	3017	2943	11
33	4	3112	3029	2	3112	2974	2	28	1	4219	3995	1	4219	3997	1
28	1	4212	4066	1	4212	3993	1								

Tab. S9: Combination modes calculated with G16 and G09 on PBE0/def2-QZVPP and def2-TZVPP level. Harmonic wavenumber ν_h, anharmonic wavenumber ν_{ah} in cm^{-1}, anharmonic infrared intensity I_{ah} in $km\,mol^{-1}$. Only listed if intensity exceeds $1\,km\,mol^{-1}$

PBE0/def2-QZVPP								PBE0/def2-TZVPP							
		G16			G09					G16			G09		
Modes		ν_h	ν_{ah}	I_{ah}	ν_h	ν_{ah}	I_{ah}	Modes		ν_h	ν_{ah}	I_{ah}	ν_h	ν_{ah}	I_{ah}
33	32	231	312	1				33	30	371	365	5	371	365	5
33	31	320	381	1				32	28	557	503	2	557	503	2
32	31	364	399	4	364	344	3	28	27	968	916	2	968	917	2
33	30	372	432	2	372	364	2	30	26	1131	1112	2	1131	1112	2
32	30	415	456	14				32	24	1186	1161	5			
32	28	549	608	1	549	497	1	33	23	1197	1168	2	1197	1167	2
28	27	963	982	2	963	911	1	29	26	1222	1200	13	1222	1201	13
30	26	1130	1130	2	1130	1112	2	31	24	1273	1239	1	1273	1239	1
32	24	1183	1195	16	1183	1155	12	32	22	1275	1244	2	1275	1244	2
29	26	1219	1218	15	1219	1200	15	33	21	1276	1247	3	1276	1247	3
33	23	1196	1224	2	1196	1166	2	33	20	1280	1249	2	1280	1248	2
31	24	1272	1263	27	1272	1238	27	29	25	1287	1263	2	1287	1263	2
28	26	1264	1274	5	1264	1205	5	32	18	1400	1365	4			
29	25	1285	1280	3	1285	1262	3	27	26	1404	1383	2	1404	1384	2
33	21	1276	1300	5	1276	1246	4	29	24	1415	1386	2	1415	1386	2
33	20	1280	1302	2	1280	1249	2	31	19	1437	1392	7	1437	1392	7
27	26	1403	1392	2	1403	1383	2	30	21	1460	1428	1	1460	1428	1
29	24	1413	1404	2	1413	1385	2	29	23	1472	1441	7	1472	1441	7
31	19	1435	1414	6	1435	1391	6	27	25	1469	1443	4	1469	1443	4
27	25	1468	1451	3	1468	1442	3	31	18	1487	1445	2	1487	1445	2
29	23	1470	1459	3	1470	1439	3	30	19	1488	1448	1	1488	1448	1
30	19	1486	1464	1				33	15	1492	1454	8	1492	1454	8
31	18	1487	1467	3	1487	1444	3	26	19	2063	2013	2	2063	2013	2
33	15	1492	1507	4	1492	1454	4	16	14	2819	2732	1	2819	2732	1
28	23	1515	1517	1	1515	1447	1	14	9	2950	2870	1	2950	2870	1
26	19	2061	2019	2	2061	2011	2	13	12	2954	2877	2	2954	2877	2
16	14	2816	2737	1	2816	2729	1	13	11	2963	2890	2			
14	13	2909	2841	1	2909	2835	1	12	11	2974	2891	2	2974	2891	2
14	9	2947	2873	1	2947	2867	1	12	10	2976	2896	3	2976	2896	3
13	12	2954	2882	2	2954	2878	2	12	9	2993	2912	41	2993	2912	41
13	11	2962	2894	2				13	9	2983	2914	4			
12	11	2973	2895	2	2973	2891	2	11	10	2986	2919	18	2986	2914	9
12	10	2976	2899	4	2976	2895	4	11	9	3002	2926	5	3002	2939	3
13	10				2965	2895	1	10	9	3005	2939	8			
12	9	2992	2918	3				28	1	4274	4054	1	4274	4057	1
11	10	2984	2918	8	2984	2916	10								
13	9	2981	2922	24											
11	9	3000	2928	4	3000	2923	2								
10	9	3003	2943	6											
28	1	4267	4114	1	4267	4052	1								

References

(S1) Lüttschwager, N. O. B. *Raman Spectroscopy of Conformational Rearrangements at Low Temperatures*; Springer International Publishing, 2014.

(S2) TURBOMOLE V7.4.1 2019, a development of University of Karlsruhe and Forschungszentrum Karlsruhe GmbH, 1989-2007, TURBOMOLE GmbH, since 2007; available from `http://www.turbomole.com`.

(S3) Dirac, P. A. M. Quantum mechanics of many-electron systems. *P. R. Soc Lond. A-Conta.* **1929**, *123*, 714–733.

(S4) Slater, J. C. A Simplification of the Hartree-Fock Method. *Phys. Rev.* **1951**, *81*, 385–390.

(S5) Vosko, S. H.; Wilk, L.; Nusair, M. Accurate spin-dependent electron liquid correlation energies for local spin density calculations: a critical analysis. *Can. J. Phys.* **1980**, *58*, 1200–1211.

(S6) Becke, A. D. Density-functional exchange-energy approximation with correct asymptotic behavior. *Phys. Rev. A* **1988**, *38*, 3098–3100.

(S7) Lee, C.; Yang, W.; Parr, R. G. Development of the Colle-Salvetti correlation-energy formula into a functional of the electron density. *Phys. Rev. B* **1988**, *37*, 785–789.

(S8) Becke, A. D. Density-functional thermochemistry. III. The role of exact exchange. *J. Chem. Phys.* **1993**, *98*, 5648–5652.

(S9) Grimme, S.; Antony, J.; Ehrlich, S.; Krieg, H. A consistent and accurate ab initio parametrization of density functional dispersion correction (DFT-D) for the 94 elements H-Pu. *J. Chem. Phys.* **2010**, *132*, 154104.

(S10) Grimme, S.; Ehrlich, S.; Goerigk, L. Effect of the damping function in dispersion corrected density functional theory. *J. Comput. Chem.* **2011**, *32*, 1456–1465.

(S11) Eichkorn, K.; Treutler, O.; Öhm, H.; Häser, M.; Ahlrichs, R. Auxiliary basis sets to approximate Coulomb potentials (Chem. Phys. Letters 240 (1995) 283-290). *Chem. Phys. Lett.* **1995**, *242*, 652–660.

(S12) Eichkorn, K.; Weigend, F.; Treutler, O.; Ahlrichs, R. Auxiliary basis sets for main row atoms and transition metals and their use to approximate Coulomb potentials. *Theor Chem Acta* **1997**, *97*, 119–124.

(S13) Weigend, F. Accurate Coulomb-fitting basis sets for H to Rn. *Phys. Chem. Chem. Phys.* **2006**, *8*, 1057.

(S14) Deglmann, P.; May, K.; Furche, F.; Ahlrichs, R. Nuclear second analytical derivative calculations using auxiliary basis set expansions. *Chem. Phys. Lett.* **2004**, *384*, 103–107.

(S15) Sierka, M.; Hogekamp, A.; Ahlrichs, R. Fast evaluation of the Coulomb potential for electron densities using multipole accelerated resolution of identity approximation. *J. Chem. Phys.* **2003**, *118*, 9136–9148.

(S16) Brandenburg, J. G.; Bannwarth, C.; Hansen, A.; Grimme, S. B97-3c: A revised low-cost variant of the B97-D density functional method. *J. Chem. Phys.* **2018**, *148*, 064104.

(S17) Bachorz, R. A.; Bischoff, F. A.; Glöß, A.; Hättig, C.; Höfener, S.; Klopper, W.; Tew, D. P. The MP2-F12 method in the TURBOMOLE program package. *J. Comput. Chem.* **2011**, *32*, 2492–2513.

(S18) Weigend, F. A fully direct RI-HF algorithm: Implementation, optimised auxiliary basis sets, demonstration of accuracy and efficiency. *Phys. Chem. Chem. Phys.* **2002**, *4*, 4285–4291.

(S19) Hättig, C.; Tew, D. P.; Köhn, A. Communications: Accurate and efficient approximations to explicitly correlated coupled-cluster singles and doubles, CCSD-F12. *J. Chem. Phys.* **2010**, *132*, 231102.

(S20) Frisch, M. J.; Trucks, G. W.; Schlegel, H. B.; Scuseria, G. E.; Robb, M. A.; Cheeseman, J. R.; Scalmani, G.; Barone, V.; Mennucci, B.; Petersson, G. A.; Nakatsuji, H.; Caricato, M.; Li, X.; Hratchian, H. P.; Izmaylov, A. F.; Bloino, J.; Zheng, G.; Sonnenberg, J. L.; Hada, M.; Ehara, M.; Toyota, K.; Fukuda, R.; Hasegawa, J.; Ishida, M.; Nakajima, T.; Honda, Y.; Kitao, O.; Nakai, H.; Vreven, T.; Montgomery, J. A., Jr.; Peralta, J. E.; Ogliaro, F.; Bearpark, M.; Heyd, J. J.; Brothers, E.; Kudin, K. N.; Staroverov, V. N.; Keith, T.; Kobayashi, R.; Normand, J.; Raghavachari, K.; Rendell, A.; Burant, J. C.; Iyengar, S. S.; Tomasi, J.; Cossi, M.; Rega, N.; Millam, J. M.; Klene, M.; Knox, J. E.; Cross, J. B.; Bakken, V.; Adamo, C.; Jaramillo, J.; Gomperts, R.; Stratmann, R. E.; Yazyev, O.; Austin, A. J.; Cammi, R.; Pomelli, C.; Ochterski, J. W.; Martin, R. L.; Morokuma, K.; Zakrzewski, V. G.; Voth, G. A.; Salvador, P.; Dannenberg, J. J.; Dapprich, S.; Daniels, A. D.; Farkas, O.; Foresman, J. B.; Ortiz, J. V.; Cioslowski, J.; Fox, D. J. Gaussian 09 Revision E.01. 2013; Gaussian Inc. Wallingford CT.

(S21) Frisch, M. J.; Trucks, G. W.; Schlegel, H. B.; Scuseria, G. E.; Robb, M. A.; Cheeseman, J. R.; Scalmani, G.; Barone, V.; Petersson, G. A.; Nakatsuji, H.; Li, X.; Caricato, M.; Marenich, A. V.; Bloino, J.; Janesko, B. G.; Gomperts, R.; Mennucci, B.; Hratchian, H. P.; Ortiz, J. V.; Izmaylov, A. F.; Sonnenberg, J. L.; Williams-Young, D.; Ding, F.; Lipparini, F.; Egidi, F.; Goings, J.; Peng, B.; Petrone, A.; Henderson, T.; Ranasinghe, D.; Zakrzewski, V. G.; Gao, J.; Rega, N.; Zheng, G.; Liang, W.; Hada, M.; Ehara, M.; Toyota, K.; Fukuda, R.; Hasegawa, J.; Ishida, M.; Nakajima, T.; Honda, Y.; Kitao, O.; Nakai, H.; Vreven, T.; Throssell, K.; Montgomery, J. A., Jr.; Peralta, J. E.; Ogliaro, F.; Bearpark, M. J.; Heyd, J. J.; Brothers, E. N.; Kudin, K. N.; Staroverov, V. N.; Keith, T. A.; Kobayashi, R.; Normand, J.; Raghavachari, K.; Rendell, A. P.; Burant, J. C.; Iyengar, S. S.; Tomasi, J.; Cossi, M.; Millam, J. M.; Klene, M.; Adamo, C.; Cammi, R.; Ochterski, J. W.; Martin, R. L.; Morokuma, K.; Farkas, O.; Foresman, J. B.; Fox, D. J. Gaussian 16 Revision A.03. 2016; Gaussian Inc. Wallingford CT.

(S22) Perdew, J. P.; Wang, Y. Accurate and simple analytic representation of the electron-gas correlation energy. *Phys. Rev. B* **1992**, *45*, 13244–13249.

(S23) Perdew, J. P.; Burke, K.; Ernzerhof, M. Generalized Gradient Approximation Made Simple. *Phys. Rev. Lett.* **1996**, *77*, 3865–3868.

(S24) Perdew, J. P.; Ernzerhof, M.; Burke, K. Rationale for mixing exact exchange with density functional approximations. *J. Chem. Phys.* **1996**, *105*, 9982–9985.